Combined *ab initio* and LEED *I*/*V* study of submonolayer adsorption of In on W(110)

Markus Stöhr* and Raimund Podloucky
Institut für Physikalische Chemie, Universität Wien, Sensengasse 8/7, A-1090 Vienna, Austria

Martin Gabl,† Norbert Memmel, and Erminald Bertel
Institut für Physikalische Chemie, Universität Innsbruck, Innrain 52a, A-6020 Innsbruck, Austria
(Received 29 June 2007; revised manuscript received 5 October 2007; published 30 November 2007)

The atomic structure of various indium adlayers at submonolayer coverages on W(110) is investigated by a density functional theory (DFT) approach as well as by analysis of low-energy electron diffraction intensities (LEED *I*/*V*). Single-atom adsorption is studied by DFT, with the result that adsorption at the pseudo-fourfold coordinated sites of the W(110) is most preferable, followed by bonding to the pseudo-threefold and twofold short-bridge sites. Both theory and experiment reveal that for the (3×1) structure, which corresponds to a coverage of 0.33 monolayer (ML), indium atoms occupy exclusively pseudo-fourfold coordinated sites, while for the (1×4) phase (0.75 ML coverage) and (1×5) phase (0.80 ML coverage), pseudo-threefold and twofold short-bridge sites are also occupied. According to DFT, the (1×4) structure is the most stable one, closely followed by the (1×5) structure. Analysis of DFT studies on free monolayers of In reveals the significant influence of In-In bonding on the formation of these adlayer structures. The low-coverage (3×1) structure is energetically the least favorable one, in agreement with the experimental finding that the (3×1) structure is only metastable and transforms with increasing time or upon annealing into islands of (1×4) patterns. In order to investigate whether the (3×1) structure might be stabilized by contaminants, DFT calculations were also performed for coadsorbing hydrogen and oxygen with indium on W(110). However, the (3×1) structure always remains metastable. Furthermore, we find that phase separated regions of oxygen patches and (1×4) In islands are stabilized by about 1 eV/atom relative to mixed (3×1) In+O configurations. This is in very good agreement with the experimental observation that the $(3\times1)\rightarrow(1\times4)$ transition can be triggered by additional oxygen.

DOI: 10.1103/PhysRevB.76.195449 PACS number(s): 68.43.Bc, 68.43.Fg, 68.43.Jk, 68.49.Jk

I. INTRODUCTION

Indium and tungsten are metals with very different physical properties. Tungsten has the highest melting point of all metals (3683 K), while indium melts already at 430 K. Indium is very soft, while tungsten is hard and brittle, in particular, when carbon and oxygen impurities are present. Due to the softness of indium, one might expect that indium likes to grow on tungsten in a pseudomorphic manner, with In atoms occupying the energetically most favorable single-atom adsorption sites, even if this requires some change of the In-In bond length as compared to the bulk. However, as will be shown in this paper, this assumption does not hold due to the rather large lattice misfit (the next-neighbor In-In distance exceeds that of tungsten by 18.6%). Furthermore, both materials adopt different crystallographic structures in their respective bulk phases. Tungsten crystallizes in the body-centered cubic structure, while indium is one of the few materials with a body-centered tetragonal structure. Due to its rather large c/a ratio of 1.52, this structure is more conveniently described as a face-centered tetragonal (fct) structure, since, in this case, the c/a ratio is close to 1 (1.08). Hence, the indium bulk structure corresponds to a face-centered cubic structure slightly elongated along the c axis. In the following, we will always use the fct notation to specify the crystallographic directions of indium.

The growth of submonolayer In films on W(110) was first investigated with low-energy electron diffraction (LEED) and work-function measurements by Gorodetskii *et al.*[1] and Boiko.[2] In these investigations as well as in the more recent combined LEED and x-ray photoelectron spectroscopy (XPS) work of Bürgener *et al.*,[3] several ordered structures were observed with increasing coverage upon room-temperature deposition: a (3×1) structure at low coverages [$\approx$0.2 monolayer (ML) according to the XPS calibration of Ref. 3], followed by (1×4) and (1×5) patterns at coverages of about 0.65 and 0.80 ML, respectively. [One complete monolayer is defined with respect to the atomic density of the W(110) surface layer, i.e., 1.41×10^{15} atoms/cm^2.] In a very recent LEED and scanning tunneling microscopy (STM) work, it was reported that the (3×1) structure is only metastable.[4] Within 1–2 h after deposition or upon annealing, the (3×1) structure transforms irreversibly into islands with a higher coverage corresponding to a (1×4) structure. This finding is in contrast to the paper of Boiko in 1990, in which the mentioned temperature-induced transition was also reported; however, it was claimed that this transition is reversible. The (3×1) and (1×4) adsorption structures (denoted as γ and α structures) were also observed for the closely related In/Mo(110) adsorbate system.[5]

In the investigations listed above, various structure models were suggested. Whereas for the low-coverage (3×1) structure all studies agree, different models were proposed for the high-coverage (1×4) and (1×5) phases. Bürgener *et al.*[3] suggest pseudomorphic long-bridge ("pseudo-fourfold") adsorption sites with intermittent empty rows, which are needed for the correct coverage. This empty space might also be convenient for reducing the compressive stress in the In

overlayer due to the compact packing into pseudomorphic sites. However, Boiko[2] as well as Gabl *et al.*[4] favored a more uniform distribution of the indium adatoms, which resembles a Moire-like structure of In(111) on W(110). In all these studies, the proposed structure models are based on visual inspections of LEED patterns only, without any quantitative analysis of the diffraction intensities. The purpose of the present work is to study these structures in a more accurate way, experimentally by a LEED I/V analysis as well as theoretically in terms of *ab initio* density functional theory (DFT) calculations. Furthermore, since DFT calculations can also provide adsorption energies, we are also able to address the stability or metastability of the various adsorbate structures for different coverages.

II. EXPERIMENTAL SETUP AND COMPUTATIONAL DETAILS

A. Experimental setup

Experiments where performed in an UHV chamber with a base pressure of 1×10^{-10} mbar equipped with standard facilities for sample preparation and a video-LEED system (Er-LEED, Specs GmbH). The W(110) surface was cleaned by annealing in 5×10^{-8} mbar of oxygen at 1550 K, followed by a flash to 2300 K. The temperature was monitored with an infrared pyrometer through a ZnSe window with an accuracy of about ±20 K. Surface cleanliness was verified by LEED and Auger electron spectroscopy.

Indium was evaporated from a Knudsen cell with a resistively heated boron-nitride crucible using deposition rates and sample temperatures of ≈0.2 ML/min and ≈330 K, respectively. Normal-incidence LEED patterns were recorded at sample temperatures below 200 K in the energy range 20–500 eV by means of a 12-bit digital camera.[6] The recorded *IV* spectra were normalized to the primary beam intensity. To further improve the quality of the data, the spectra of symmetrically equivalent beams were averaged and slightly smoothed. For pure W(110), a data set of eight beams with a total energy width of 2740 eV was evaluated. For the (3×1)-In/W(110) structure, the data set consists of nine integral and ten fractional order beams with integrated energy widths of 2915 and 3595 eV, respectively, while for the (1×4) and (1×5) structures, sets of eight integral and ten fractional (ΔE=2740 eV+4014 eV) and nine integral and nine fractional (ΔE=2880 eV+3165 eV) order beams, respectively, were used.

LEED intensities were calculated using the TensErLEED program package.[7] In the tensor-LEED approach, first, a full dynamical calculation is carried out for a certain reference structure and then intensity changes due to small deviations from this reference are calculated by a perturbation scheme.[8–10] A semiautomated structural search is made by a frustrated simulated annealing procedure,[11] guided by the Pendry *R*-factor R_P (Ref. 12) for the quantitative comparison of experimental and calculated spectra. The real part of the inner potential (defined relative to the vacuum energy), V_{0r}, was allowed to be energy dependent according to $V_{0r}=V_{00}+\max(-0.03-77.07/\sqrt{\text{Energy/eV}+17.79};-10.84)$ eV, with V_{00} adapted in the course of the theory-experiment fit. The imaginary part of the inner potential was chosen as $V_{0i}=-6(\text{Energy}/230\ \text{eV})^{1/3}$ eV in order to obtain the correct energy dependence of the electron attenuation length with a minimum around 50 eV.

Seventeen relativistically calculated, spin averaged phase shifts were used for W and In, respectively, as provided by Ref. 13. Special care was taken not to leave the validity range of the perturbation ansatz. This was checked by a full dynamical recalculation of the intensities for the optimized geometry.

Statistical error limits for the varied parameters were estimated by the variance of the Pendry *R*-factor,[12] $\text{var}(R_P)=R_{P,min}\sqrt{8V_{0iP}/\Delta E}$, with $R_{P,min}$ the minimum *R*-factor and $V_{0i}\approx5$ eV the magnitude of the average imaginary part of the inner potential as also used for the calculation of R_P. All structures with *R*-factors below $[R_{P,min}+\text{var}(R_P)]$ are supposed to be within the limits of error. Typically, errors are in the range 2–5 pm.

B. Computational aspects

For the DFT calculations, we used the Vienna *ab initio* Simulation Package[14,15] (VASP) with the projector augmented wave implementation.[16,17] The exchange-correlation functional was approximated within the generalized gradient approximation as parametrized by Perdew, Burke, and Ernzerhof (PBE; this abbreviation will be used further on to indicate our calculated results).[18] A plane wave basis set with an energy cutoff of 350 eV was used. Suitable **k**-point grids were constructed according to Ref. 19: a $13\times13\times13$ mesh for the primitive bulk unit cell and a $13\times13\times1$ mesh for the surface slabs were chosen. For larger unit cells, the **k**-point grids were scaled down accordingly. For the Brillouin zone integration, the smearing method of Ref. 20 with a width of 0.1 eV was applied. The In 4*d* and W 5*p* semicore states are treated as valence states. For the geometrical relaxation, the Hellman-Feynman forces were minimized within a quasi-Newton algorithm and a convergency criterion of being smaller than 0.01 eV/Å. Symmetric slabs with 7, 9, 11, and 13 layers of W and with different vacuum spacings were tested in order to find the optimized number of layers for the larger-scale calculations. Finally, the chosen setup for the adsorption studies was a symmetric slab with seven W layers with coverages of 0.33/0.75/0.80 ML of indium. A vacuum region equivalent to five W(110) bulk layers (≈11 Å) was added. Within this setup, the calculations are sufficiently converged and the numerical errors of adsorption energies and related quantities are less than 10^{-2} eV.

III. RESULTS

A. Clean W(110)

As a first test of our computational approach, we derived the lattice parameters and the bulk moduli of the bulk phases of In and W (Table I). For W, our calculated values of 3.189 Å and 315 GPa agree reasonably well with the experimental values of 3.165 Å and 314 GPa, respectively. Using a local density approximation (LDA) of the exchange-

TABLE I. Experimental and DFT derived bulk moduli, lattice constants, and surface energies for W and In.

	W		In	
B [GPa]	315[a]	314[b]	40.5	42.4[c]
a [Å]	3.189[a]	3.165[d]	4.68	4.60[d]
c/a			1.06	1.08[d]
		E_{surf} (J/m^2)		
(100)	3.99[a]	4.635[e]	0.36	0.560[e]
(110)	3.25[a]	4.005[e]	0.37	0.592[e]
(111)	3.54[a]	4.452[e]	0.32	
(001)			0.31	0.488[e]

[a]Our results.
[b]Experiment (Ref. 22).
[c]Experiment (Ref. 23).
[d]Experiment (Ref. 24).
[e]DFT (Ref. 25).

correlation functional rather than PBE, we obtain 3.13 Å and 344 GPa, in very good agreement with the established theoretical values of Jansen and Freeman[21] of 3.15 Å and 345 GPa. The agreement of the LDA values with the experimental data is slightly less favorable than for the PBE calculation. Therefore, the generalized gradient PBE approach was then applied further on, which is of particular importance for calculating adsorption energies, because the overbinding effect of LDA might lead to rather large errors.

For In, we calculated the fct lattice constant of $a=4.68$ Å, the c/a ratio of 1.06, and the bulk modulus of 40.5 GPa. All these values are in good agreement with the experimental values of $a=4.60$ Å, $c/a=1.08$, and $B=42.4$ GPa, respectively. The small bulk modulus of In, which is about ten times lower than for W, indicates the softness of the indium metal.

Surface energies were derived from the differences of the total energy E_{slab} for the relaxed surface slab consisting of N layers, and of the total energy of N bulk layers with energy E_{bulk},

$$E_{surf} = \frac{1}{2}(E_{slab} - NE_{bulk}). \quad (1)$$

Because the slab has two equivalent surfaces, the differences are divided by 2. The results are listed in Table I and compared to existing calculated data.

Similar to the bulk moduli, the surface energies of W (ranging from 3 to 4 J/m^2) and In ($\approx$0.3 J/m^2) differ by about a factor of 10. As expected from simple bond-cutting arguments, the surface energy per atom is smallest for the surfaces with the closest packing [i.e., E_{surf} for W(110) =1.44 eV/atom and E_{surf} for In(111)=0.19 eV/atom] and largest for surfaces with the maximum number of broken bonds [i.e., E_{surf} for W(111)=4.01 eV/atom and E_{surf} for In(110)=0.38 eV/atom]. Correspondingly, the bond-cutting model of Methfessel *et al.*[26] reproduces our calculated values within an accuracy of $\approx$20% or better. Comparing our PBE data to the earlier LDA calculations of Vitos *et al.*[25] (Table I), we find that our values are smaller by $\approx$20% for W and by $\approx$30% for In, respectively, which indicates the overbinding effect of LDA. However, the orientation dependence of surface energies is the same for both calculations.

TABLE II. Comparison of first-layer relaxation for W(110) as obtained by various experimental and theoretical methods.

Method	$\Delta d_{12}/d_{bulk}$ (%)	Ref.
Experiment		
LEED	0.0±3.0	27
High energy ion scattering	<2	28
Photoelectron diffraction	0.0±1.0	29
LEED	−3.0±0.6	30
LEED	−3.0±1.3	31
LEED	−1.8±1.3	Present work
Theory		
Tight-binding	−1.4	32
Equivalent crystal theory	−2.1	33
Tight-binding	−5.0	34
LDA (seven-layers)	−3.3	30
PBE (seven-layers)	−3.7	Present work

Results for clean W(110) for the first-layer relaxation $\Delta d_{12}/d_{bulk}$ are compared in Table II. As expected, for all studies, a contraction of the first-layer distance is observed. Experimental values range from 0 to 3%. Our value of 1.8%, being somewhat lower than the values from recent LEED studies, is still within the experimental error bars. All studies agree that relaxations of the second and deeper layers were found to be insignificant.

Overall, calculated contractions of the first-layer distance vary between 1.4% and 5%. However, the result of the present work as well as of the most recent other DFT calculations are about 3.5%; the precise values are weakly dependent on the thickness of the chosen tungsten slab.[30] In agreement with experiment, our calculation yields only a small expansion of the second-layer distance of $\approx$0.5%.

For an easier comparison between experimental and theoretical structural data, theoretically calculated distances of surface structures as listed in the remaining part of this paper are rescaled in order to reproduce the experimental bulk lattice constant of tungsten.

B. Single-atom adsorption

For studying the adsorption properties of single In atoms, a (4×4) unit cell (dashed line in Fig. 1) with one In atom per cell was chosen. Because of the large unit cell, the In-In distances are so large that In-In interactions can safely be neglected. Adsorption energies E_{ad} per In atom for a unit cell with n_{In} In atoms were calculated as the difference per In atom of the total energy of the final relaxed configuration E_{slab} minus the sum of the total energy of the clean tungsten surface E_{W} and n_{In} times the total energy of the In atom E_{In}^{atom},

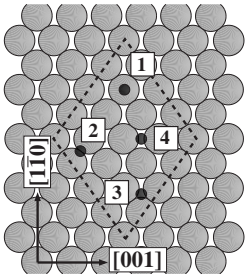

#	name	E_{ad} [eV/atom]
4	"4-fold hollow"	-2.99
3	"3-fold hollow"	-2.91
2	short bridge	-2.75
1	on-top	-2.62

FIG. 1. Principal adsorption sites and their adsorption energies of single In atoms on W(110).

$$E_{ad} = (E_{slab} - E_W - n_{\mathrm{In}} E_{\mathrm{In}}^{atom})/n_{\mathrm{In}}. \quad (2)$$

The four principal adsorption sites and their adsorption energy are illustrated in Fig. 1.

Because of its lowest energy of E_{ad}=−2.99 eV/atom, the long-bridge site is the most favorable adsorption location. It can also be considered as a pseudo-fourfold hollow site, a notation which we will use further on in order to point out its high coordination. The most unfavorable position is the single-coordinated on-top site with an energy of E_{ad}= −2.62 eV/atom. The energies of the two other adsorption sites, the pseudo-threefold hollow and (short) bridge sites, are in between these two extremal values. It should be noted that the threefold site adsorption is not stable because lateral forces drive the In atom toward the pseudo-fourfold site. The adsorption energy of E_{ad}=−2.91 eV/atom in Fig. 1 was derived by constraining the lateral coordinates of the In atom (i.e., the distance to all three neighbors is fixed) and by only allowing ionic relaxation in the direction normal to the surface.

The calculated cohesive energy of the solid In phase is −2.40 eV/atom. In Eq. (2), by replacing the total energy of a free In atom E_{In}^{atom} by the total energy of In in the bulk phase, we obtain −0.59 and −0.22 eV/atom for the fourfold hollow and on-top adsorption sites, accordingly. These negative energies indicate that In submonolayers wet the W(110) surface rather than form three-dimensional agglomerates, which is in agreement with experiment.

Furthermore, surface alloying is highly improbable: the calculated energy for creating a vacancy on W(110) is ≈10 eV, whereas placing In at the vacancy site yields an adsorption energy of ≈−5 eV. In other words, exchanging a surface W atom by In atom costs ≈5 eV.

The lowest energy path for an isolated In adatom from the fourfold site to the next similar site includes the twofold (short) bridge position as a saddle point. From that, the diffusion barrier may be estimated as the energy difference between the twofold bridge and fourfold site, resulting in a diffusion barrier of 0.24 eV. Assuming a prefactor of 10^{13} s^{-1}, this barrier is equivalent to an adatom hopping rate of 10^{10} hops per second at 500 K, or a diffusion coefficient

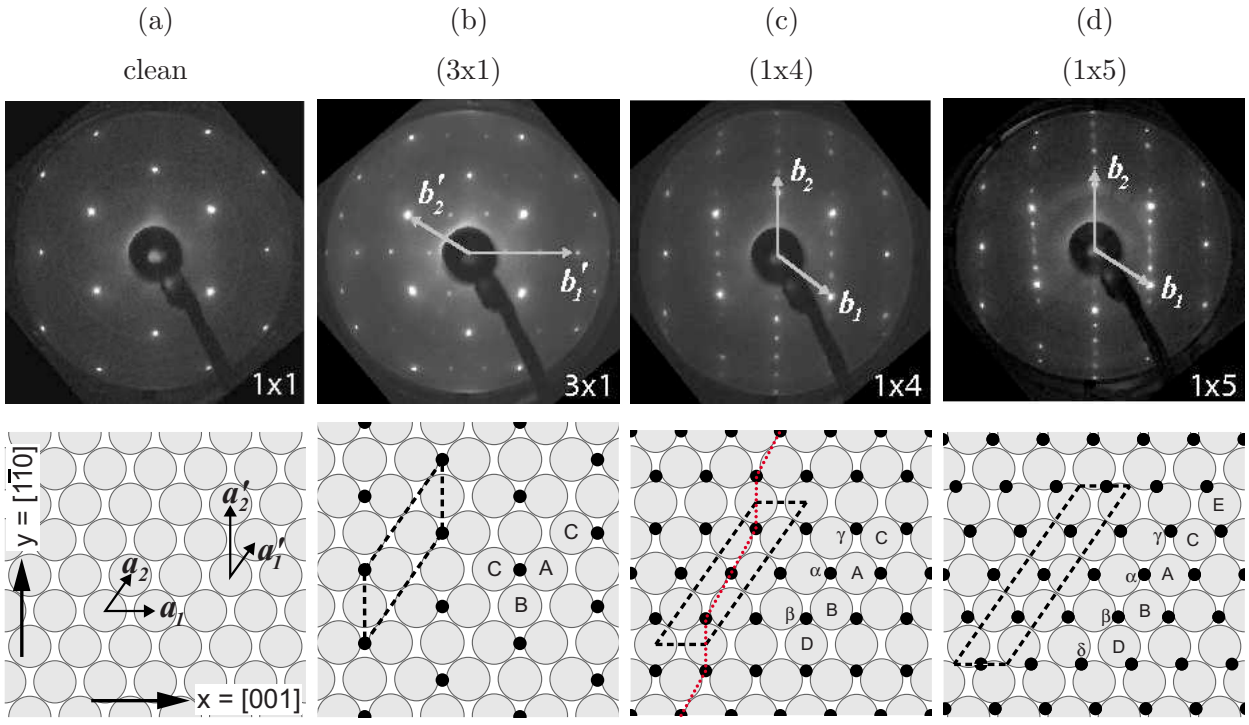

ideal (exp.) coverage	0.33 (0.20) ML	0.75 (0.65) ML	0.80 (0.80) ML
E_{ad} [eV/atom]	-3.03	-3.31	-3.24

FIG. 2. (Color online) LEED patterns and top-view structural models for clean W(110) and (3×1), (1×4), and (1×5) In structures. Note that the (3×1) supercell is specified relative to the basis vectors a_1' and a_2' of W(110), whereas the other structures are specified with respect to the basis vectros a_1 and a_2. Greek letters denote In; Latin letters denote W.

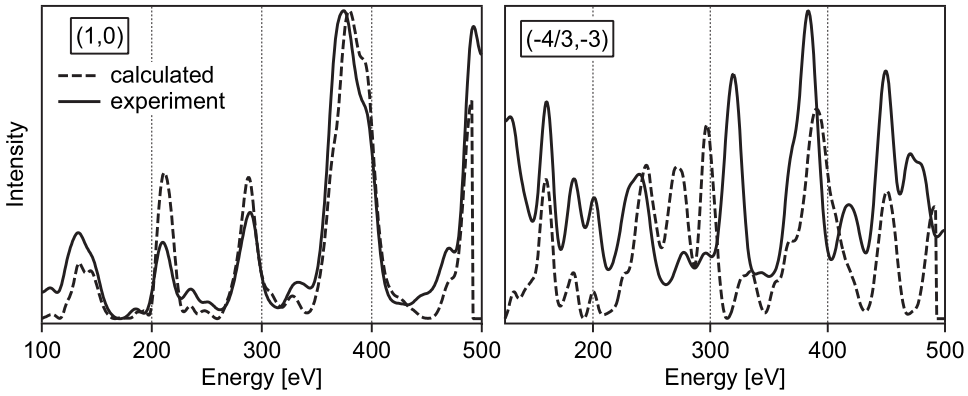

FIG. 3. Comparison of experimental and simulated LEED intensities for the (1,0) and the $(-4/3,-3)$ diffraction spots of the (3×1) overlayer.

of 3×10^{-9} m^2 s^{-1}, respectively. This is about 1 order of magnitude higher than the experimental value of 2×10^{-10} m^2 s^{-1} as reported by Trzcinski *et al.*[35] There are two main reasons for the apparent discrepancy: First, Trzcinski *et al.* measured the diffusion coefficients at finite coverages, whereas our calculation is for isolated adatoms. Second, the experiment yields a macroscopic diffusion coefficient (i.e., for diffusion lengths well exceeding typical terrace widths, thus including diffusion events over steps), while we deal with diffusion on flat terraces only.

C. 3×1

For low coverages, a (3×1) superstructure is observed by LEED [top of Fig. 2(b)]. The LEED pattern corresponds to a real-space unit cell, with unit cell vectors along the $[1\bar{1}1]$ (long side) and the $[1\bar{1}0]$ (short side) directions of the W(110) lattice, as shown in the lower part of the figure. XPS studies of Bürgener *et al.* reveal a coverage of about 0.2 ML for this structure. We assume adsorption of one In per unit cell, which corresponds to 0.33 ML for a full coverage. Each unit cell consists of three W surface atoms (large gray circles) and one In atom (small black circles).

As for the single-atom adsorption, DFT finds that the preferred adsorption site in the (3×1) structure is the fourfold hollow site with an adsorption energy −3.03 eV per In atom. Note that this value is very close to the adsorption energy (−2.99 eV) of single In atoms (see Fig. 1), as one might have already guessed from the rather large In-In distance of 448 pm in the (3×1) structure, which is significantly larger than the next-neighbor distance of 331 pm in bulk In.

In order to determine the adsorption sites from experiment, TensErLEED calculations were carried out with In atoms in the four principal adsorption sites. Only relaxations of In and W atoms along the surface normal were allowed at this stage. In agreement with the theoretical predictions, we find that the fourfold hollow site is favored with a Pendry *R*-factor of 0.36. For the threefold hollow, bridge, and on-top sites, the *R*-factor amounts to 0.42, 0.49, and 0.47 (see Table III). Since the variance of the Pendry factor is small $[\mathrm{var}(R_P)=0.019]$, the latter three adsorption sites can clearly be excluded. The preference for the fourfold site is particularly manifested if only the superstructure-induced fractional order spots are considered ($R_P=0.58$ versus $R_P\geq0.72$), although the *R*-factors of the fractional spots are quite large on an absolute scale.

TABLE III. Pendry *R*-factors for different adsorption sites (relaxation of atomic positions only along the *z* direction).

	Fourfold hollow	Threefold hollow	Bridge	On-top
R_P (all)	0.36	0.42	0.49	0.47
R_P (int)	0.24	0.25	0.32	0.31
R_P (fract.)	0.58	0.72	0.75	0.75

Once the adsorption sites were determined, the structure was further optimized by allowing also for lateral relaxations of surface W atoms and by considering suboptimal coverage (i.e., free tungsten patches on the surface), which reduces the minimum Pendry *R*-factor to 0.28 for the fourfold hollow site. Examples of experimental and simulated $I(E)$ spectra are shown in Fig. 3. The detailed geometry parameters as obtained from both experiment and DFT theory are listed in Table IV. In experiment as well as in the calculations, it is found that In pushes W atoms next to it [labeled "A" and "C" in Fig. 2(b)] slightly sidewards by 3 pm and also downwards by 2 pm, resulting in shorter In-W distances.

For symmetry reasons, the W atom labeled "B" in Fig. 2(b) does not shift laterally, but only relaxes normal to the surface. LEED and PBE derive an outward displacement of 4 and 5 pm, respectively (see Table IV); thus, the distance to the next In adatom is slightly reduced.

The distance between the In adlayer and the center of the buckled surface layer of W(110) amounts to 233 pm (LEED) and 235 pm (PBE). This corresponds to a contraction of about 6% of the nearest-neighbor In-W distance as compared with a hard-sphere model making use of the atomic sizes. Compared to clean W(110), the average interlayer distance d_{12} is slightly altered by In adsorption (LEED: −3.1%, PBE: −2.4%). Changes in deeper layers are within the error limits of our LEED analysis (≈3 pm).

D. 1×4

At coverages of about 0.65 ML, a (1×4) diffraction pattern is observed by LEED,[3] from which a unit cell with three In atoms and four W atoms (corresponding to an ideal coverage of 0.75 ML) is derived. In the adlayer, In atoms are

TABLE IV. LEED and PBE results for the (3×1)-In/W(110) structure. The atoms are labeled according to Fig. 2(b). Displacements Δz are defined with respect to the center of the W surface layer. All values are given in pm.

	d_{In}	d_{12}	d_{23}	Δx_A	Δx_B	Δx_C	Δz_A	Δz_B	Δz_C
LEED	233	218	224	+3	0	−3	−2	+4	−2
PBE	235	220	225	+3	0	−3	−2	+5	−2

tightly packed, with an atom density being even 2% larger than that of an In(111) bulklike layer.

The structural model as obtained from the PBE calculations is shown in Fig. 2(c). It places one of the In atoms (labeled α) in the energetically most favorable fourfold hollow site and the other two In atoms (labeled β and γ) into positions close to the pseudo-threefold sites. In the calculation, it turns out that the β and γ atoms are arranged symmetrically to the fourfold coordinated site.

On one hand, from the adsorption energies calculated for single In atoms, adsorption in fourfold hollow sites are preferable. On the other hand, this would result in a strong compression by 18% of In distances along the $[1\bar{1}1]$ direction as compared with the nearest-neighbor bulk distance. Since the adsorption energy in the threefold site differs by less than 0.1 eV from that of the fourfold site, adsorption of the In atoms in or close to the pseudo-threefold site provides a reasonable compromise between optimum chemical adsorption and large stress within the In adlayer. Compared to the (3×1) structure, the overall bonding is strengthened because the averaged adsorption energy per In atom in the (1×4) overlayer amounts to −3.31 eV/atom.

Guided by the theoretical results, the LEED analysis was performed in the following way: in a first coarse grid search, the position of In atom α was kept fixed in a fourfold coordinated site, while the positions of the remaining two In atoms β and γ were arranged symmetrically to the α atom along a line moving away from the next fourfold site along $[1\bar{1}0]$. Then, in a second step close to the minimum of the grid search, positions were fine-tuned using the tensor-LEED approach. Figure 4 shows the variation of the *R*-factor as the position of the indium atoms β and γ is changed in the first step of the evaluation. As can be seen, adsorption of all indium atoms (α, β, and γ) in pseudomorphic fourfold sites, which is essentially the model suggested by Bürgener *et al.*,[3] clearly has to be excluded. Rather, the optimum adsorption site almost perfectly matches the ideal threefold position. It should be mentioned that in the LEED analysis, the presence of clean tungsten patches was also considered, since the (1×4) structure exists over a rather large coverage range.[4]

Final parameter optimization reveals the following details (see also Table V): the optimum positions of In atoms β and γ are on the high-symmetry line along $[1\bar{1}0]$ running through a fourfold site, 62 pm (PBE: 65 pm) away from the fourfold site, which is just slightly beyond the threefold coordinated position. They are located 248 pm (PBE: 254 pm) above the center of the W surface layer. In contrast, In atom α in the fourfold site lies deeper, namely, 242 pm (PBE: 249 pm) above the W top layer, resulting in buckling of 6 pm (PBE: 5 pm). Compared to the (3×1) structure, the In atom in the fourfold site is located 11 pm (PBE: 14 pm) higher above the top tungsten layer, indicating that some In-W interlayer bonding strength is exchanged against intralayer In-In bonding. Due to the denser In overlayer in the (1×4) structure, also the average W interlayer distance d_{12} is increased toward the bulk interlayer distance.

Drawing a line that indicates the alignment of the In adatoms [dotted line in Fig. 2(c)], it can be seen that within the unit cell this line is tilted away from the unit cell vector. As a consequence, kinks in this interconnecting line appear from unit cell to unit cell with a period of 890 pm along $[1\bar{1}0]$. These kinks are also the reason for the striped structure observed by STM for (1×4) islands of In/W(110) (Ref. 4): the measured corrugation of these stripes is ≈8 pm, which compares well with the buckling in the In overlayer (6 pm) as described above. The buckling of the W surface layer is quite small, close to the experimental and theoretical accuracies (LEED: 4 pm, PBE: 2 pm). Lateral displacements of W surface atoms as well as displacements of deeper-layer atoms out of their bulk positions are found to be insignificant (below 1 pm) for both LEED and PBE.

E. 1×5

The unit cell of the (1×5) structure is similar to that of the (1×4) structure, but elongated by 25% along $[1\bar{1}1]$. For

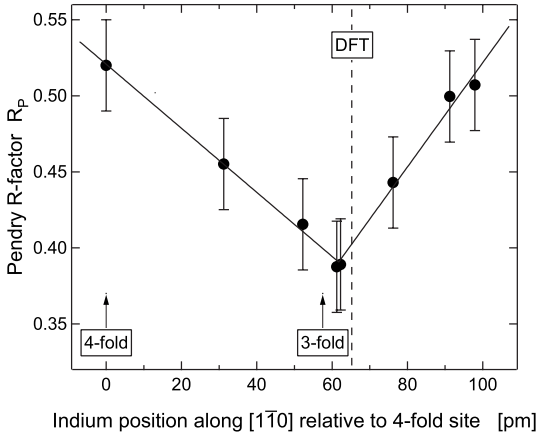

FIG. 4. LEED analysis of the (1×4) structure. In atom α was fixed at the fourfold site, while atoms β and γ were displaced symmetrically along a line moving away from the next fourfold site adsorption site along $[1\bar{1}0]$. The diagram shows the Pendry *R*-factor as a function of In positions along this line. The vertical dashed lines indicate the position favored by PBE.

TABLE V. Interlayer distances and positions of In and W surface atoms as obtained by LEED and DFT (PBE) for (1×4)-In/W(110). Atoms are labeled according to Fig. 2(c). x and y coordinates of In are given relative to the closest fourfold adsorption site. Displacements Δz are defined with respect to the center of the In and W surface layers. All distances are given in pm.

	d_{In}	d_{12}	d_{23}	Δx_α	Δx_β	Δx_γ	Δy_α	Δy_β	Δy_γ	Δz_α	Δz_β	Δz_γ	Δz_A	Δz_B	Δz_C	Δz_D
LEED	246	222	224	0	0	0	0	−62	62	−4	2	2	−2	−2	2	2
PBE	252	222	225	0	1	2	0	−65	65	−3	2	2	−1	0	1	1

the analysis, a unit cell with four In atoms and five W surface atoms was constructed, in perfect agreement with the experimentally determined coverage of 0.80 ML.[3]

The calculated structure as shown in Fig. 2(d) shows similarities to the (1×4) case, but now the higher coverage of 0.80 ML of In atoms has to be accommodated. Similar to the (1×4) phase, one In atom (α) sits in the fourfold site and two In atoms (β, γ) close to the threefold coordinated site.

For the fourth In atom in the unit cell (labeled δ), no such optimal adsorption site is available and it has to adsorb at the less favorable short-bridge site (cf. Fig. 1).

Due to the occupation of this unfavorable adsorption site, the average adsorption energy is slightly reduced to −3.24 eV/atom as compared to the (1×4) structure with −3.31 eV/atom. Furthermore, the buckling is increased from 6 to 23 pm (PBE: 17 pm). Because of the buckling, the compressive stress in the In adlayer is reduced: a coverage of 0.80 ML corresponds already to an In atom density which exceeds that of a densely packed In(111) layer by 8%.

The rather complex (1×5) structure was verified experimentally by taking the theoretically calculated structure as a starting point for the analysis of the LEED I/V data and searching for the optimum parameters in the vicinity of the theoretically predicted positions using the tensor-LEED approach. This yields a minimum R-factor $R_P=0.39$, almost the same as obtained in the analysis of the (1×4) structure. Theoretically and experimentally determined geometric parameters are listed in Table VI. In general, calculation and experiment agree well with each other. In particular, in both cases, we find that when compared to the (1×4) structure, the In atoms β and γ in the pseudo-threefold positions move ≈17 pm closer to the α atom as a consequence of forcing the In atom δ into the short-bridge site. Furthermore, the In atoms no longer reside on the high-symmetry line running through a W surface atom along $[1\bar{1}0]$ (i.e., $|\Delta x|>0$). Due to adsorption of In in the short-bridge site, the buckling of the W(110) surface layer is approximately twice as much as for the (1×4) case (both in experiment and theory). However, the buckling is still quite small (LEED: 7 pm, PBE: 3 pm).

IV. DISCUSSION

A. Comparison of overstructures

The basic properties of the three In adlayer structures (interlayer distances d_{ij}, layer bucklings b_j, and adsorption energies) as determined by LEED and PBE are summarized in Table VII. In general, it can be stated that the agreement between experimental and theoretical data is very good.

The In layer in the (3×1) structure is unbuckled, since all atoms reside in equivalent quasi-fourfold site coordinated adsorption sites. In the (1×4) phase, the In atoms occupy two different adsorption sites, resulting in a finite buckling of the In layer. However, the buckling is still small (6 pm) as also expected from a simple hard-sphere model. For the (1×5) overlayer, the buckling is considerably increased due to occupation of the twofold short-bridge site. Buckling of the tungsten top layer is in the range 3–7 pm for all three structures.

For the (3×1) structure, the distance between the centers of the indium adlayer and the W surface layer exceeds the W(110) interlayer distance by $\approx4\%$ due to the larger size of the In atoms as compared to W. For the (1×4) and (1×5) structures, the layer distance is increased significantly to $\approx11\%$ and $\approx12\%$, respectively, indicating a weakening of In-W bonds in favor of a stronger coupling within the In adlayer. This weakening of the In-W bond strength becomes even clearer when calculating the energy required for separating the (3×1), (1×4), and (1×5) layers from the surface. The binding energies per indium atom for freestanding (3×1), (1×4), and (1×5) layers are −0.81, −1.93, and −1.97 eV, respectively (see Fig. 5). Thus, separating the (3×1) layer costs 2.22 eV per In atom, whereas for the (1×4) and (1×5) phases, only 1.38 and 1.27 eV, respectively, are required. Finally, we note that the surface relaxation of W(110) is reduced upon In deposition from $\approx3\%$ to $\approx1.5\%$ for the (1×4) and (1×5) superstructures.

Inspection of the calculated adsorption energies as listed in Table VII reveals that the (1×4) structure is energetically the most stable one. The (1×5) structure is slightly less

TABLE VI. LEED and PBE results for the (1×5)-In/W(110) structure. Atoms are labeled according to Fig. 2(d). x and y coordinates of the In atoms are given relative to the closest fourfold adsorption site. Displacements Δz are defined with respect to the center of the In and W surface layers. All distances are given in pm.

	d_{In}	d_{12}	d_{23}	Δx_α	Δx_β	Δx_γ	Δx_δ	Δy_α	Δy_β	Δy_γ	Δy_δ	Δz_α	Δz_β	Δz_γ	Δz_δ	Δz_A	Δz_B	Δz_C	Δz_D	Δz_E
LEED	247	221	224	0	−11	11	79	0	−45	45	114	−8	−4	−4	15	−5	0	0	2	2
PBE	256	222	225	0	−8	8	80	0	−50	50	113	−6	−2	−2	11	−2	0	0	1	1

TABLE VII. Interlayer distances d_{ij} and layer bucklings b_j as well as adsorption energies for In adlayers on W(110).

	(3×1)		(1×4)		(1×5)	
	LEED	PBE	LEED	PBE	LEED	PBE
			$\Delta d_{ij}/d_{bulk}$ (%)			
d_{In}	+4.9	+4.4	+9.9	+11.9	+10.0	+13.5
d_{12}	−3.1	−2.4	−0.9	−1.6	−1.1	−1.6
d_{23}	0.0	0.2	0.0	+0.0	0.0	+0.0
			b_j (pm)			
In			6	5	23	17
W_1	6	6	4	2	7	3
R_P	0.28		0.38		0.39	
E_{ad} (eV/atom)		−3.03		−3.31		−3.24

stable since it requires occupation of the less favored bridge site. The destabilization of the (3×1) structure is much stronger by 0.28 eV/atom although all In atoms occupy the most favorable fourfold site hollow site. Hence, the destabilization of the (3×1) structure is a consequence of the large In-In separation and the associated loss of In-In bonding strength.

B. Freestanding monolayers

In order to emphasize the importance of the In-In intralayer bonding, we also calculated the binding energy of freestanding (3×1), (1×4), (1×5), and (1×1) In monolayers and compared them to freestanding monolayers corresponding to the low-index surfaces of indium. The binding energy is defined according to Eq. (2), taking again the total energy of a free indium atom as reference energy. In Fig. 5, the calculated binding energies are plotted versus the atomic densities of the various monolayers. The data exhibit a parabolic relationship, with a minimum at an areal atom density of 109% relative to that of an In(111) monolayer, which is close to the density of the (1×5) structure. The compression to a density beyond that of the densest In bulk layer obviously occurs in order to compensate for the missing bonds on both sides of the freestanding layer. Adsorption on W(110) partially relaxes this compression and the (1×4)—with an areal density still slightly larger than on In(111)—is favored over the (1×5) structure.

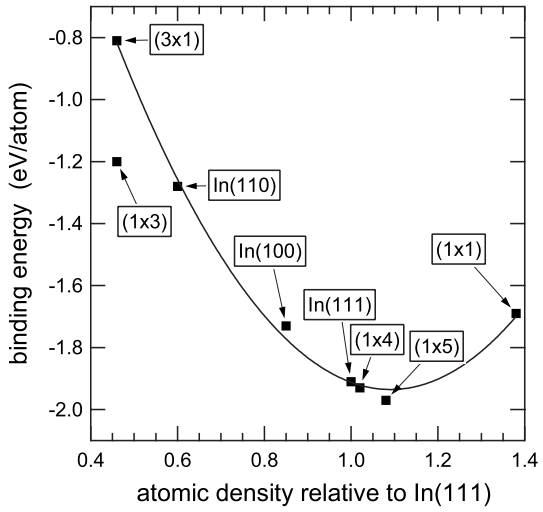

FIG. 5. Binding energy vs atom density for freestanding In monolayers in various geometries. For more details, see text.

The scaling of binding energy with atomic density as the only important parameter is only possible, since all monolayers considered so far are relatively weakly anisotropic, even in the In(110) structure. For strongly anisotropic films, the simple relationship does not hold. For example, the data point denoted "(1×3)" at a relative density of 0.46 lies well below the parabola spanned by all other data points. It was obtained for a structure where In atoms are arranged in densely packed rows along [001], which are separated from each other by two empty rows. This structure will be discussed in more detail below.

C. Molecular dynamics

Molecular dynamics simulations were performed in order to confirm that the derived (1×4) structure is indeed the thermodynamical ground state for an ideal coverage of 0.75 ML. We used a (4×4) unit cell with initial on-top positions for the In atoms, which certainly is an energetically very unfavorable configuration [Fig. 6(a)]. Equilibrating the system at $T=1000$ K for 5 ps and cooling it down to 400 K for another 5 ps result in a configuration as illustrated in Fig. 6(b). The distribution of In atoms is already very similar to the (1×4) structure [Fig. 2(c)] as calculated before. Relaxing this last structure further at $T=0$ K finally leads to the configuration in Fig. 6(c), which is exactly the (1×4) adstructure.

The preference for the (1×4) structure can also be understood from rather simple epitaxial considerations. The W(110) surface has a quasihexagonal symmetry. Therefore, the growth of In layers with a similar surface symmetry, i.e.,

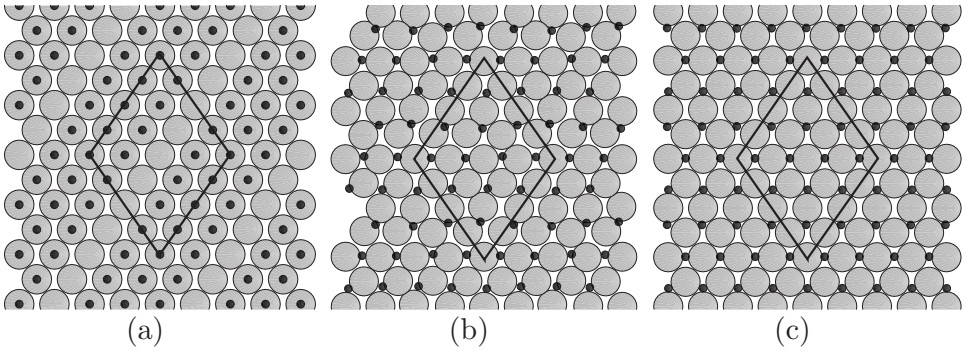

FIG. 6. Molecular dynamics simulations of 0.75 ML In/W(110) with a (4×4) unit cell. (a) Starting configuration, (b) cooled system, and (c) relaxed structure. W atoms, large gray circles; In atoms, small black circles.

with a (111) orientation, is most likely, in particular, since this is also the most densely packed In layer. Furthermore, in order to minimize the misfit between the W(110) and In(111) planes, at least along one direction, the orientation of In$[1\bar{1}0]$ parallel to W[001] is advantageous, since the misfit along these directions is only 2% (see Fig. 7). This corresponds to the Nishiyama-Wassermann orientation for epitaxial growth. However, along W$[1\bar{1}1]$, the misfit is considerable ($\approx$23%). Nevertheless, almost perfect coincidence can be achieved after four tungsten unit cells or three indium unit cells, respectively, if the In(111) unit cell is slightly distorted by 6.5°, such that the cell angles of W(110) and the distorted In(111) layer are equal to each other. By such a construction, the (1×4) structure with three In atoms per unit is obtained.

D. Metastability of (3×1)

The higher stability of the high-coverage (1×4) phase as compared to the low-coverage (3×1) structure implies that the (3×1) structure is only metastable and that the energy of In/W(110) can be minimized by forming islands with a local (1×4) structure. This conclusion is in line with our previous LEED and STM experiments, showing that within several hours after deposition or upon annealing, the (3×1) structure transforms into islands of (1×4). Obviously, the (3×1) structure can only be observed due to kinetic restrictions. However, in view of the calculated low diffusion barrier of 0.24 eV (cf. Sec. III B), this is somewhat surprising. By using a prefactor of 10^{13} s^{-1}, this barrier is equivalent to an adatom hopping rate of 10^9 hops/s at room temperature; thus, single In adatoms should be mobile enough to travel across the surface and to agglomerate into (1×4) islands. The energy barrier of 0.24 eV as mentioned above is for single isolated indium adatoms. Selected representative migration paths for other coverages were calculated as well by applying the nudged elastic band method as implemented in VASP (Ref. 36) within a two-dimensional supercell. Its basic lattice vectors were three times larger than the vectors of the standard unit cell. Choosing the (3×1) structure as a starting point, an In atom was moved along the $[1\bar{1}1]$ direction. This type of migration might be a preliminary step to finally build up the (1×3) structure. The associated energy barrier for this movement was calculated as $\approx$0.1 eV, which is less than half the barrier for an isolated In adatom. Other starting setups were tested as well, but always resulted in energy barriers of $\approx$0.1 eV when In moved closer to other In atoms. In comparison to the single-atom case, barrier heights, in general, are strongly reduced. From an energetic point of view, these very small barrier heights indicate a very fast transition from (3×1) to other more stable structures. A possible explanation for this apparent puzzle is that small (1×4) islands are rather unstable and decay before further adatoms are attached. In terms of nucleation kinetics, the latter scenario would be equivalent to a critical island size substantially larger than 1. Furthermore, the degeneracy of the different structures may play a role for the growth of the different adlayer domains. The (3×1) structure can grow on three possible sublattices, while the (1×4) structure can grow on four sublattices. This might reduce the growth exponent for the (1×4) domains relative to that for the (3×1) domains, thus slowing down growth of the (1×4) domains.[37] However, as the growth exponent is independent of temperature, this argument should hold at all temperatures—in contrast to experiment where spontaneous formation of the (1×4) phase is observed at higher deposition temperatures. Thus, degeneracy as the only reason for the formation of the (3×1) structure at low temperatures can be ruled out.

Triggered by the instability of the (3×1) structure, we also searched for alternative adsorption structures for a coverage of 0.33 ML. As it turned out, even if islanding is forbidden, the (3×1) structure is not the energetically most favorable structure at that coverage. Rather, a (1×3) structure, consisting of single [001]-oriented rows of In atoms (located in fourfold hollow sites) separated by two empty [001] rows, is lower in energy. It has an adsorption energy of −3.18 eV/atom, which is in between the adsorption energies of the (3×1) and (1×4) structures. The reason for the higher stability of the atomic chains of the (1×3) structure

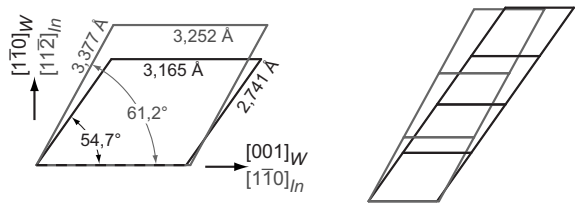

FIG. 7. Relationship between the W(110) (black lines) and the In(111) unit cell (gray lines) in a Nishiyama-Wassermann orientation. The left panel shows both unit cells in direct comparison. The right panel demonstrates that supercells consisting of four tungsten or three indium unit cells, respectively, are close to coincidence.

as compared to the (3×1) structure is a strong gain in In-In interaction energy due to the closer packing of In atoms, at least along one direction, which outweighs the loss of In-In interaction due to an increased distance in the perpendicular direction. However, since these atomic chains are already building blocks of the (1×4) structure, their formation may be hindered for the same reasons as for the formation of (1×4) islands themselves. Furthermore, once the conditions (e.g., temperature) are such that the (1×3) structure can be formed, the system is probably also able to directly convert to the even more stable (1×4) phase, thus explaining why the (1×3) chain structure has never been observed in experiment.

The arguments given above attribute the existence of the (3×1) structure to a kinetic stabilization relative to the (1×3) and (1×4) structures. Another possibility, which should be critically examined, is the influence of contaminants. Hence we also calculated the adsorption properties of hydrogen and oxygen on clean and In-covered W(110). Hydrogen was investigated as it is always present in the UHV rest gas, but is difficult to detect when adsorbed. Oxygen was investigated since it was used extensively in the preparation of clean W(110) and since we observed a pronounced influence on the $(3\times1)\rightarrow(1\times4)$ transition in experiment.[4] The adsorption of oxygen and hydrogen on clean W(110) has been studied experimentally in a number of publications (Refs. 38–40, 30, and 41, respectively). For both species, the threefold coordinated adsorption site was found to be the energetically most favorable one. We confirm this favorite adsorption site and calculate adsorption energies of ≈-1.5 and ≈-4.2 eV/atom for single H and O atoms. One additional hydrogen atom within the (3×1) and (1×3) unit cells increases the difference in adsorption energies between these two structures, i.e., H contamination does not stabilize the (3×1) structure with respect to the (1×3) structure.

Calculation of the adsorption energies for the (3×1) and (1×3) structures with one or two preadsorbed oxygen atoms reveals that the relative stability of the (1×3) and (3×1) structures remains the same. O atoms stick to their favorite threefold hollow site, even in the presence of In. Since the In-O distance is small (≈1.5 Å), a repulsive interaction pushes the In atoms away from the fourfold hollow site. Consequently, the adsorption energy of the In atoms is lowered with respect to the oxygen-free surface. For high coverages (in our calculations, this corresponds to a concentration of 66 at. % additional O atoms), the adsorption energy of In turns even lower than the cohesive energy of its bulk configuration, i.e., layer growth is hindered in this case and growth of three-dimensional In islands has to be expected.

The total adsorption energy of In and O atoms for the $(3\times1)+$O configurations is about 1 eV/atom less favorable than separated areas of pure O and pure In (1×4) structures. This is substantially more than the 0.3 eV/atom difference between the (3×1) and (1×4) structures (see Table VII). Hence, oxygen adsorption increases the driving force for the formation of the (1×4) structure, in accordance with our experimental observation that exposure to oxygen triggers the transition from the (3×1) structure (with low local In coverage) into (1×4) islands with high local In coverage.[4] Thus, the present PBE calculations are in perfect agreement with our experimental findings not only with respect to the structural data, but also with respect to the energetics [metastability of (3×1)] and the driving forces for the (3×1) to (1×4) transition. However, there is a clear discrepancy of our present data (both experimental and theoretical) to a previous study of Boiko,[2] which reports that the $(3\times1)\Leftrightarrow(1\times4)$ transition is reversible with respect to coverage and temperature. In the following, we will consider two scenarios to explain this discrepancy.

The simplest explanation for the different experimental observations would be that in our experiments, the sample was cooled too fast (we partially used liquid nitrogen cooling), thus freezing the high-temperature (1×4) phase and overlooking the reversibility of the transition. However, even in experiments without liquid nitrogen cooling, the transition from (1×4) back to (3×1) was never observed. Furthermore, a transition from (1×4) to (3×1) upon lowering the temperature is in disagreement with the PBE results: The (1×4) structure is the energetically most favorable structure. Thus, according to the laws of thermodynamics, the (1×4) rather than the (3×1) structure should be formed upon temperature reduction, in contradiction to the results of Boiko.

The second scenario involves some unknown contamination which stabilizes the (3×1) structure. (However, as already discussed above, neither hydrogen nor oxygen will do this.) Upon heating, the adsorbates desorb and the system transforms to the (1×4) phase. If subsequent cooling is done rapidly with low background pressure, then the (1×4) structure still remains, while upon slow cooling with a bad background pressure, the system might readsorb the contaminants and return to the (3×1) structure. A drawback of this scenario is its failure to explain why at room temperature the system transforms to the (1×4) structure with increasing time, although contamination increases rather than decreases with time.

None of these two scenarios gives a satisfactory and consistent explanation of all experimental and theoretical data. Thus, although we were able to shed some light onto this problem, the (meta)stability of the (3×1) In/W(110) phase is still an open problem.

ACKNOWLEDGMENTS

Financial support by the Austrian Science Fund (FWF) within the Joint Research Program S90 and the Science College W4 is gratefully acknowledged. We thank W. Meyer and L. Hammer (University of Erlangen-Nürnberg) for supporting the LEED I/V calculations.

*markus.stoehr@univie.ac.at
†martin.gabl@uibk.ac.at

[1] D. Gorodetskii, A. Yas'ko, and Fung-Kho, Izv. Akad. Nauk USSR, Ser. Fiz. **33**, 467 (1969).
[2] B. Boiko, Phys. Chem. Mech. Surf. **5**, 1054 (1990).
[3] M. Bürgener, A. Bukaluk, M. Cyrankiewicz, A. Goldmann, R. Siuda, and M. Trzcinski, Surf. Sci. **529**, 490 (2003).
[4] M. Gabl, M. Trzcinski, N. Memmel, A. Bukaluk, and E. Bertel, Surf. Sci. **600**, 4390 (2006).
[5] A. Katoh, H. Miwa, Y. Maehara, H. Kawanowa, and Y. Gotoh, Surf. Sci. **566**, 181 (2004).
[6] Sensicam, pCO Computer Optics, Kelheim, Germany.
[7] V. Blum and K. Heinz, Comput. Phys. Commun. **134**, 392 (2001).
[8] P. J. Rous, J. B. Pendry, D. K. Saldin, K. Heinz, K. Muller, and N. Bickel, Phys. Rev. Lett. **57**, 2951 (1986).
[9] P. Rous and J. Pendry, Surf. Sci. **219**, 355 (1986).
[10] P. Rous, Prog. Surf. Sci. **39**, 3 (1992).
[11] M. Kottcke and K. Heinz, Surf. Sci. **376**, 352 (1997).
[12] J. Pendry, J. Phys. C **13**, 937 (1980).
[13] W. Meyer and K. Heinz (private communication).
[14] G. Kresse and J. Hafner, Phys. Rev. B **47**, 558 (1993).
[15] G. Kresse and J. Furthmüller, Phys. Rev. B **54**, 11169 (1996).
[16] P. E. Blöchl, Phys. Rev. B **50**, 17953 (1994).
[17] G. Kresse and D. Joubert, Phys. Rev. B **59**, 1758 (1999).
[18] J. P. Perdew, K. Burke, and M. Ernzerhof, Phys. Rev. Lett. **77**, 3865 (1996).
[19] H. J. Monkhorst and J. D. Pack, Phys. Rev. B **13**, 5188 (1976).
[20] M. Methfessel and A. T. Paxton, Phys. Rev. B **40**, 3616 (1989).
[21] H. J. F. Jansen and A. J. Freeman, Phys. Rev. B **30**, 561 (1984).
[22] F. H. Featherston and J. R. Neighbours, Phys. Rev. **130**, 1324 (1963).
[23] B. S. Chandrasekhar and J. A. Rayne, Phys. Rev. **124**, 1011 (1961).
[24] N. Ridley, J. Less-Common Met. **8**, 354 (1965).
[25] L. Vitos, A. Ruban, H. Skriver, and J. Kollar, Surf. Sci. **411**, 186 (1998).
[26] M. Methfessel, D. Hennig, and M. Scheffler, Appl. Phys. A: Solids Surf. **55**, 442 (1992).
[27] M. Lagally, J. Buchholz, and G. Wang, J. Vac. Sci. Technol. **12**, 213 (1975).
[28] R. J. Smith, C. Hennessy, M. W. Kim, C. N. Whang, M. Worthington, and Xu Mingde, Phys. Rev. Lett. **58**, 702 (1987).
[29] B. Kim, J. Chen, J. L. Erskine, W. N. Mei, and C. M. Wei, Phys. Rev. B **48**, 4735 (1993).
[30] M. Arnold, G. Hupfauer, P. Bayer, L. Hammer, K. Heinz, B. Kohler, and M. Scheffler, Surf. Sci. **382**, 288 (1997).
[31] G. Teeter, J. L. Erskine, F. Shi, and M. A. Van Hove, Phys. Rev. B **60**, 1975 (1999).
[32] J. S. Luo and B. Legrand, Phys. Rev. B **38**, 1728 (1988).
[33] A. Rodriguez, G. Bozzolo, and J. Ferrante, Surf. Sci. **289**, 100 (1993).
[34] W. Xu and J. Adams, Surf. Sci. **319**, 45 (1994).
[35] M. Trzcinski, A. Bukaluk, A. Goldmann, and M. Bürgener, Vacuum **74**, 157 (2004).
[36] H. Jonsson, G. Mills, and K. W. Jacobsen, Surf. Sci. **324**, 305 (1995).
[37] M. Tringides, in *The Chemical Physics of Solid Surfaces*, edited by D. A. King and D. P. Woodruff (Elsevier, New York, 1994), Vol. 7, pp. 215–254.
[38] P. K. Wu, M. C. Tringides, and M. G. Lagally, Phys. Rev. B **39**, 7595 (1989).
[39] M. C. Tringides, Phys. Rev. Lett. **65**, 1372 (1990).
[40] R. X. Ynzunza, R. Denecke, F. J. Palomares, J. Morais, E. D. Tober, Z. Wang, F. J. GarcÃa de Abajo, J. Liesegang, Z. Hussain, M. A. Van Hove, and C. S. Fadley, Surf. Sci. **459**, 69 (2000).
[41] M. Altman, J. W. Chung, P. J. Estrup, J. M. Kosterlitz, J. Prybyla, D. Sahu, and S. C. Ying, J. Vac. Sci. Technol. A **5**, 1045 (1987).